Review of Scientific Instruments

Design and test of a compact beam current monitor based on a passive RF cavity for a proton therapy linear accelerator

Cite as: Rev. Sci. Instrum. **92**, 113304 (2021); https://doi.org/10.1063/5.0062509
Submitted: 06 July 2021 • Accepted: 21 October 2021 • Published Online: 12 November 2021

F. Cardelli, A. Ampollini, G. Bazzano, et al.

Review of Scientific Instruments | ARTICLE | scitation.org/journal/rsi

Design and test of a compact beam current monitor based on a passive RF cavity for a proton therapy linear accelerator

Cite as: Rev. Sci. Instrum. 92, 113304 (2021); doi: 10.1063/5.0062509
Submitted: 6 July 2021 • Accepted: 21 October 2021 •
Published Online: 12 November 2021

F. Cardelli,[1] A. Ampollini,[2] G. Bazzano,[2,a)] P. Nenzi,[2] L. Piersanti,[1] C. Ronsivalle,[2] and L. Picardi[2]

AFFILIATIONS

[1] INFN Laboratori Nazionali di Frascati, Via Enrico Fermi 54, Frascati (RM) 00044, Italy
[2] ENEA C. R. Frascati, Via Enrico Fermi 45, Frascati (RM) 00044, Italy

[a)] Author to whom correspondence should be addressed: giulia.bazzano@enea.it

ABSTRACT

In a medical accelerator, real-time monitoring systems of the beam and dose delivered to the patient are mandatory. In this work, we present a compact current profile detector that has been designed and tested in the framework of the TOP-IMPLART (Intensity Modulated Proton Linear Accelerator for RadioTerapy) project. This project foresees the realization of a proton linear accelerator, currently under construction at ENEA Frascati, for proton therapy applications. The linac produces a pulsed proton beam with 3 μs duration at 50 Hz repetition rate with a pulse current between 0.5 and 50 μA. A large dynamic range and spatial constraints make the use of usual noninterceptive beam diagnostics unfeasible. Therefore, the use of a beam current monitor based on a passive RF cavity working in the TM010 mode has been proposed. This paper reports the electromagnetic design of the device guided by a simplified analytical model. A prototype of such a device has been realized, characterized, and tested on the linac with a 35 MeV beam varying the beam current. The test results in air and in vacuum, together with the signal detection systems used, are presented.

I. INTRODUCTION

Nowadays, proton therapy with cyclotrons or circular accelerators is a widely used technique for the treatment of tumors. Thanks to their distinctive interaction with human tissues, protons deliver most of their energy at the end of their path in a medium; hence, using a magnetic scanning system and varying the proton beam energy, it is possible to conform the dose to the tumor area, sparing the healthy tissues. TOP-IMPLART (Intensity Modulated Proton Linear Accelerator for RadioTherapy)[1] is a project funded by Regione Lazio (Italy) devoted to demonstrate the feasibility of a linear solution for proton therapy. The project foresees the construction of a compact fully linear proton accelerator, currently in the phase of manufacturing, assembly, and commissioning at the ENEA Frascati Research Center. The linac is a compact RF normal conducting accelerator composed of a commercial 7 MeV injector operating at 425 MHz, realized by Hitachi's AccSys, followed by a 2997.92 MHz booster composed of Side Couple Drift Tube Linac (SCDTL) modules up to 71 MeV and Coupled Cavity Linac (CCL) modules up to the final output design energy of 150 MeV.

The part of the booster presently in operation provides a beam with a peak pulse current ranging between 0.5 and 50 μA at a maximum repetition rate of 50 Hz (to be upgraded to the design repetition frequency of 100 Hz).[2] Whereas the typical average currents required for proton therapy are very low (a few nA corresponding to a few μA in the pulse), the availability of a wider current range makes the linac a suitable proton source for the test of FLASH radiotherapy. This promising new technique[3] relies on beam delivery at ultrahigh dose rates and requires high currents and high repetition rates. Otherwise, out of the medical field, it could be exploited for the radiation testing of components, material, and detectors, which typically require high particle fluxes.[4,5]

The most important parameter in medical applications is the dose delivered to the patient, which is monitored by a Dose Delivery System (DDS), independent from the accelerator and typically implemented as a set of ionization chambers. The peculiar

pulsed structure of a proton linac beam and its wide range of pulse intensities require an extended dynamic range of the monitoring devices and a detailed understanding of any potential dose-rate effect.[6]

The dose-rate stability in pulsed linacs is obtained by control of the pulse charge. The charge monitor device must therefore be non-destructive and capable to operate at the pulse repetition frequency. Traditional devices used for charge measurements in accelerators are current monitors, whose output is integrated (electronically or numerically) to compute the charge. The most common devices are current transformers, strip-lines, capacitive buttons, and wall current monitors, to cite some.[7]

In the TOP-IMPLART case, both commercially available and in-house manufactured AC current transformers are already employed both in the injector and in the booster section to monitor the beam transmission and the accelerated current. Such devices, however, while adequate in the commissioning phase, when the machine is operated at the highest available current levels, do not offer sufficient accuracy in the real-time monitoring of very low current beams (<10 μA), which are relevant for clinical applications. We therefore investigated the possibility to add a new device in the available space between the two accelerating modules, capable of covering the whole current dynamic range.

To this aim, a passive RF resonant cavity satisfying the requirements of the TOP-IMPLART accelerator has been developed. These devices are used in radiofrequency accelerators for beam current and macro-bunch charge measurements.[8] The proton beam passing along the axis through the gap of a cavity, resonating at the correct frequency, excites an electromagnetic field in it. The amplitude of this field is directly bound to the beam current intensity. Therefore, using a magnetic pickup on the outer wall of the cavity coupled to the field, it is possible to obtain a signal proportional to the beam current.

This paper is organized in two parts: the first part describes the design procedure based on 3D electromagnetic numerical calculations and Particle In Cell (PIC) simulations guided by a simplified analytic model, the cavity that has been constructed, and the results of the measurements on RF bench; the second part reports the results of the characterization tests of the response of the cavity mounted at the output of the fourth accelerating module with a 35 MeV beam. In this section, the detection system is described and the detector readings are compared with those obtained with the current diagnostics already installed on the linac.

II. DESIGN AND RF CHARACTERIZATION

A. Main requirements and principle of operation

The TOP-IMPLART linac is a sequence of RF pulsed linear accelerating modules. Figure 1 shows the layout of the segment up to 71 MeV consisting of a low frequency injector at 425 MHz composed of a Radio Frequency Quadrupole (RFQ) up to 3 MeV and a Drift Tube Linac (DTL) up to 7 MeV and a high frequency (2997.92 MHz) booster composed of eight SCDTL modules grouped in two four-module sections, each one powered by a 10 MW peak power klystron. Short Permanent Magnet Quadrupoles (PMQs) placed in the space between two accelerating tanks provide beam transverse focusing. The macropulse temporal structure is a sequence of pulses with a length variable up to 4 μs at a maximum design repetition frequency of 100 Hz. The output current can be varied from 0.5 to 50 μA by varying the voltage on an einzel lens placed inside the injector.

The typical diagnostic tools used for the commissioning of the first section of the linac before the installation of the SCDTL-5 module are described in detail in Ref. 2. They include two different types of diagnostics optimized for different current ranges: the first type provides detectable signals for beam currents in the range of 5–50 μA and is based on noninterceptive (current transformer) and interceptive (Faraday cup) monitors. The second type is used for the detection of lower intensities, which are typical of radiobiology and radiotherapy applications, and is based on detectors for radiation dosimetry (ionization chambers). However, before the installation of the second group of four SCDTL modules, it was considered necessary for monitoring and control of the accelerator to introduce after SCDTL-4 a nondestructive diagnostic, operating under vacuum, compact enough to allow the insertion of the permanent quadrupoles and able to cover the whole dynamic range of beam current intensities.

With this aim, a solution based on a passive cavity working in the TM010 mode, with a resonant frequency tuned at the repetition frequency of the micro-bunches, has been designed.

The operation principle employs the oscillations induced in the cavity by the harmonic content of the beam. In a simplified model, the particle beam can be modeled as a train of equally spaced Gaussian bunches with the period equal to the linac RF period.

According to Ref. 9, the peak power extracted from the cavity coupler can be expressed as

$$P = (I_{b0}B)^2 R_s T^2 \frac{\beta}{1+\beta^2}\cos^2\varphi, \tag{1}$$

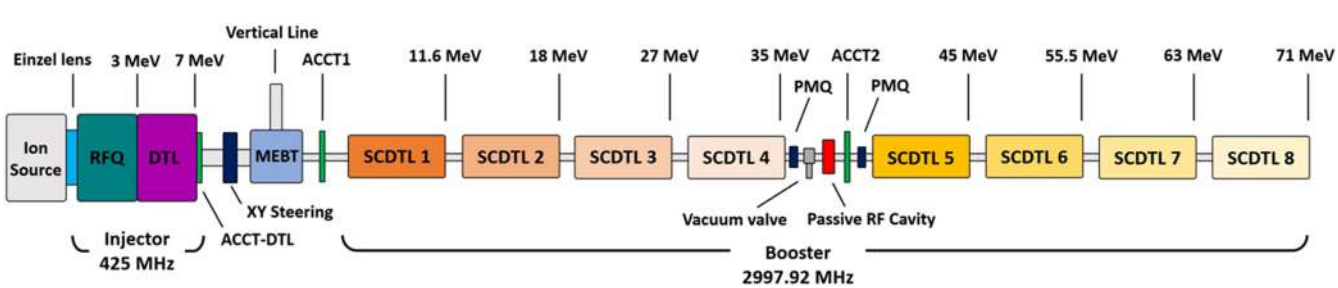

FIG. 1. TOP-IMPLART layout up to 71 MeV.

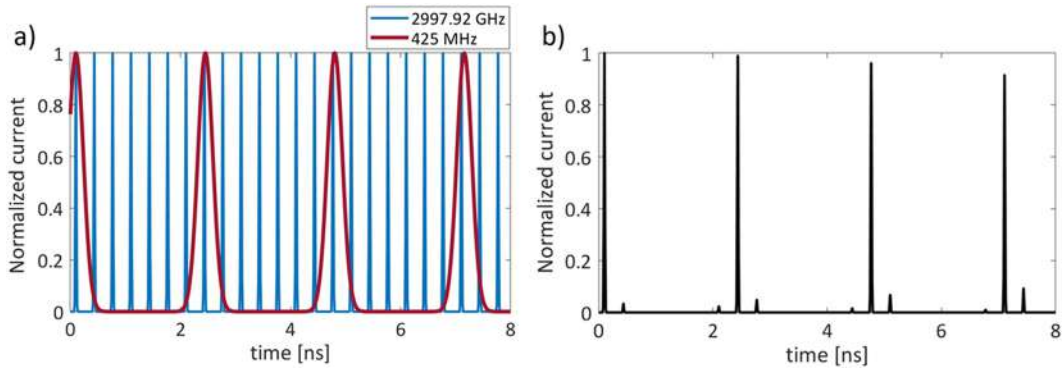

FIG. 2. (a) Simulation of temporal superposition of the injector (red) and booster phase acceptance (blue) current pulses and (b) micro-bunch amplitude modulation at the output of the booster in an 8 ns time window.

where I_{b0} is the average current amplitude; Rs is the shunt impedance of the cavity, defined as $R_s = V^2/2P_{loss}$, which measures the effectiveness of producing a voltage V for a given power P_{loss} dissipated on the cavity wall; β is the coupling coefficient of the cavity probe; and T is the cavity transit time factor. The parameter B is a form factor, which depends on the temporal shape of the micro-bunch. For a Gaussian bunch train, it is[9]

$$B = e^{-\left(\frac{\omega_b^2 \sigma_t^2}{2}\right)}, \tag{2}$$

where ω_b is the repetition rate and σ_t is the bunch length. Finally, the $\cos^2 \varphi$ term takes into account the cavity detuning with respect to the repetition frequency of bunches,[9]

$$\cos^2 \varphi = \frac{1}{[1 + 4Q_{load}^2(\Delta f / f_0)^2}. \tag{3}$$

This term gives a constraint to the model regarding the resonant frequency of the TM010 mode, which must be equal to the operating frequency of the linac. If the two frequencies differ from each other, i.e., $\Delta f \neq 0$, the pickup output signal will be attenuated and distorted.

However, the actual micro-bunch temporal structure of the TOP-IMPLART beam is not really represented by an ideal sequence of Gaussian pulses. It is mainly due to the different RF working frequencies used by the injector (425 MHz) and the booster (2997.92 MHz). As the two frequencies are not phase locked, an amplitude modulation of the micro-bunches accelerated by the booster is generated due to a slippage between the bunch injected and its driving RF pulse. Before the injection into the booster, each bunch has a periodicity of 2.35 ns and covers three RF periods due to the lengthening of the injected bunch in the 1.6 m long medium energy transfer line (MEBT). If the injector working frequency had been set at the seventh sub-harmonic of the booster RF, the resulting output beam structure would have been composed of three bunches out of seven filled with different charge contents, with a constant pattern throughout each 3 μs macropulse. However, due to the phase slippage between 425 MHz and 2.997 92 GHz, the pattern of micro-bunches shows an amplitude modulation at the residual $\approx$23 MHz frequency (i.e., 7*425–2997.92 MHz). This does not generate a pulse-to-pulse instability because the wide macropulse length allows covering several periods of the phase slippage; a pulse-to-pulse intensity reproducibility of 3% at all current levels was actually demonstrated at 35 MeV and reported in Ref. 2. A sketch of the micro-bunch amplitude variation in four RF periods, as retrieved through a simplified model of the longitudinal beam dynamics where Gaussian shapes were used for both injector bunch and booster phase acceptance, is shown in Fig. 2.

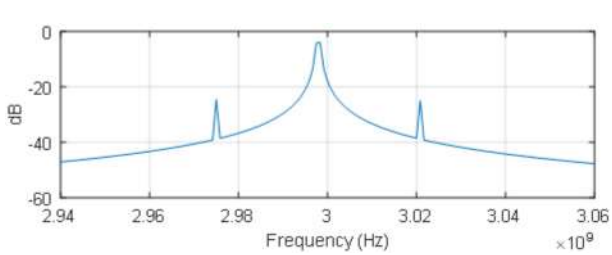

FIG. 3. Calculated FFT of the proton beam pulse.

Figure 3 shows the computed spectral analysis of the modeled beam pulse of 1 μs duration in terms of FFT; in addition to the component at 2997.92 MHz, two lateral bands separated by ±22.92 MHz, corresponding to the difference between 2997.92 and 2975 MHz, that is, the seventh harmonic of the injector operating frequency, can be seen.

III. ELECTROMAGNETIC DESIGN

The cavity geometry was designed performing a 3D computational model using the CST software. A reentrant cavity shape has been adopted, which has a higher efficiency with respect to the classic pillbox.[10] In Fig. 4, we report the simplified geometry of the cavity used for initial 3D calculations in CST. The length of the cavity (L) is fixed by the total available space in the machine layout, which is constrained by the fact that the passive RF cavity has to be inserted between two SCDTL structures, limiting debunching and particle losses; to this end, the length L of the passive cavity was set to 12 mm. The beam pipe radius (a) has been set equal to the overall machine beam pipe. The cavity radius (b) has been regulated in every

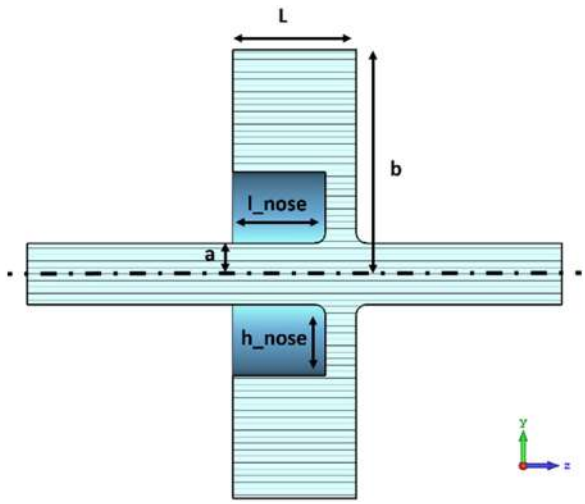

FIG. 4. Simplified model of the cavity with the principal geometric parameters.

simulation step to tune the mode TM010 at the correct working frequency. The other cavity geometrical dimensions and, in particular, the reentrant nose dimensions have been varied, optimizing the principal parameter of the cavity R_s, R_s/Q_0, and T. Due to the relatively low beta of the particles (0.266 at 35 MeV), the optimization leads to a short gap size of 3 mm, giving a transit time factor equal to 0.89. In order to maximize the output signal power, a high loaded quality factor is needed. Nevertheless, this parameter is linked to the filling (or emptying) time of the cavity $\tau = 2Q_{load}/\omega$, and this value has to be much lower than the macropulse length in order to correctly read the average current and beam charge.

Table I shows the final dimensions of the cavity. The particle beam passing through the cavity gap at the resonant frequency excites an electromagnetic field proportional to the beam current intensity. The spatial configuration of the field corresponds to the TM010 mode. Therefore, after the passage of a bunch, an oscillating azimuthal magnetic field is induced into the cavity volume. The internal conductor of a coaxial cable bent on itself can be used to realize a coupling loop, whose area is placed orthogonally to the magnetic field component. Consequently, an oscillating voltage, proportional to the beam current, will be induced at the loop terminal.

TABLE I. Geometrical parameters of the reentrant cavity.

Parameter	Unit	Value	Definition
L	mm	12	Cavity length
b	mm	21.03	Cavity radius
a	mm	3	Beam pipe radius
l_nose	mm	9	Nose length
h_nose	mm	9	Nose height

With the aim to have an accurate cavity modeling, the magnetic pickup and a rod, for frequency tuning, have been integrated into the computational model in CST (see Fig. 5). The pickup insertion (l_probe) in the cavity and its orientation with respect to the field lines determine the coupling coefficient β that has been tuned for matching the critical coupling condition (β = 1) where no reflection occurs. The RF simulation results after pickup tuning are reported in Fig. 6.

This 3D model has also been used to assess the consistence with the analytical formulation results. In particular, using the PIC module of CST code, we performed a simulation of the cavity with a passing through proton beam. The beam model structure implemented in the simulation was a train of Gaussian bunches with σ_t = 8.5 ps bunch length with a repetition frequency equal to 2997.92 MHz. For each simulated beam current, we identified the output power value as the square of the stationary voltage computed by CST. An example of such an output is reported in Fig. 7(a). In Fig. 7(b), we show the comparison between the results obtained from Eq. (2), inserting the parameter obtained from previous electromagnetic simulation of the cavity, and the power extracted from the cavity as computed by the numerical PIC simulations with the particle beam for different values of the average beam current.

The simulation results are in good agreement with the analytical model and give an estimation of the power range of the signal to be monitored and processed.

IV. HIGH ORDER MODES

Numerical computations have been carried out to evaluate if higher order modes produced by the bunch train could be excited

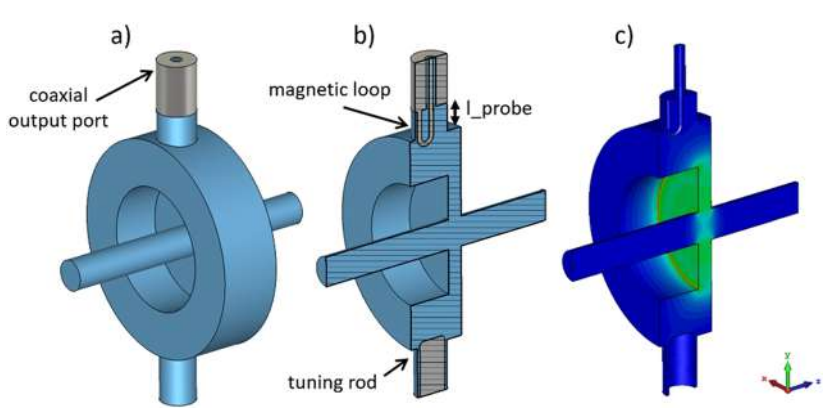

FIG. 5. Simulated cavity model (a) and (b) and electric field for the TM010 mode (c).

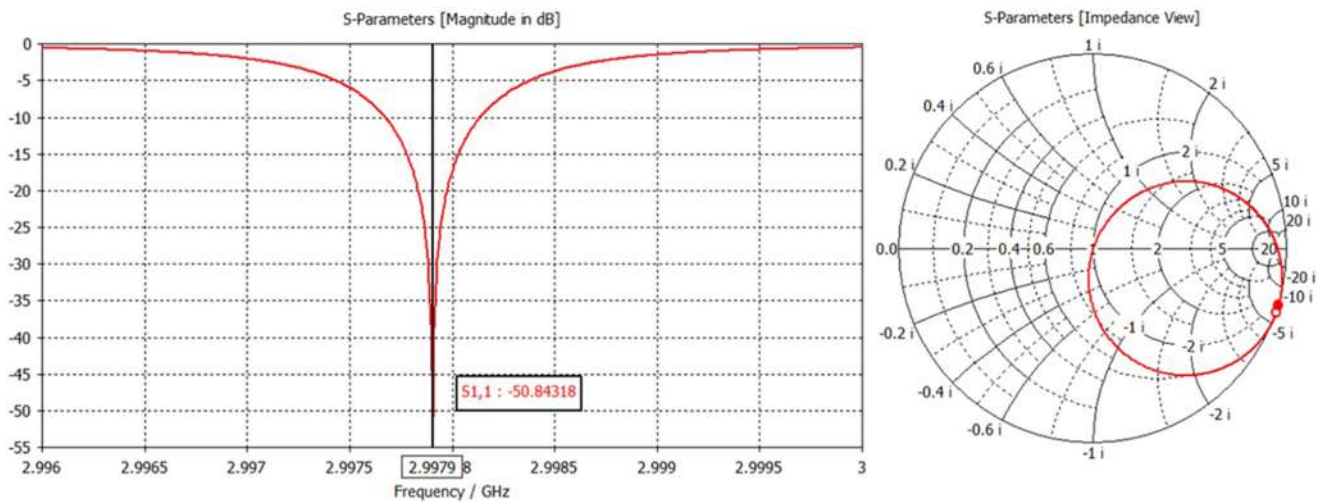

FIG. 6. Simulated scattering reflection coefficient S11 (left) and corresponding Smith chart (right).

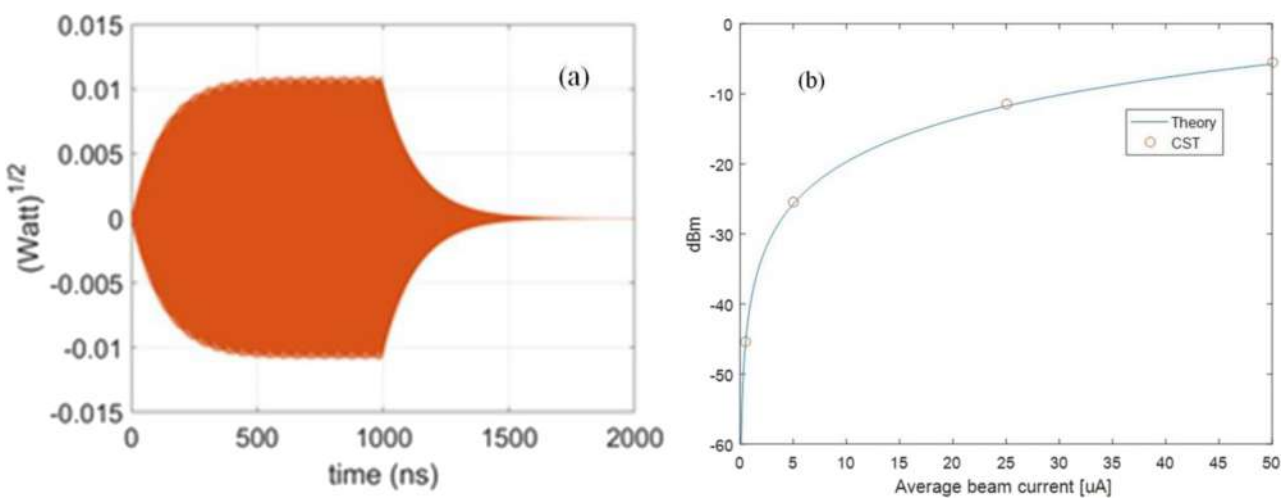

FIG. 7. (a) CST output: square root of power extracted from the cavity port as a function of time. (b) RF output power variation with respect to the beam current as computed with the PIC module simulation (CST) and the analytical model of Eq. (1) (theory).

and picked up in the measurements. The first high order mode that shows an electromagnetic pattern with an axial electric field is the TM020 at 11.66 GHz (Table II). However, this frequency is not a multiple of the fundamental of the beam spectrum, and the coupling loop is computed to be largely over-coupled to this mode ($\beta = 7$), thus giving a negligible contribution in the extracted power. In addition, this potential contribution is further suppressed at the electronic detection system level (Sec. III), whose nominal bandwidth is 0.01–8 GHz.

TABLE II. List of the computed resonant models (CST eigenmode solver).

Frequency (GHz)	Q	Type
2.997 9	4257	TM010
6.642 6	1712	TE120
10.174	4829	TE220
11.659 51	5377	TM020

V. PROTOTYPING AND CHARACTERIZATION

Relying on the electromagnetic design, a real vacuum prototype has been realized in oxygen-free high-conductivity (OFHC) copper. The mechanical drawing, including the magnetic pickup and the tuner, is shown in Fig. 8.

The design foresees the installation of the cavity prototype between the fourth and fifth SCDTL structures. The cavity has been

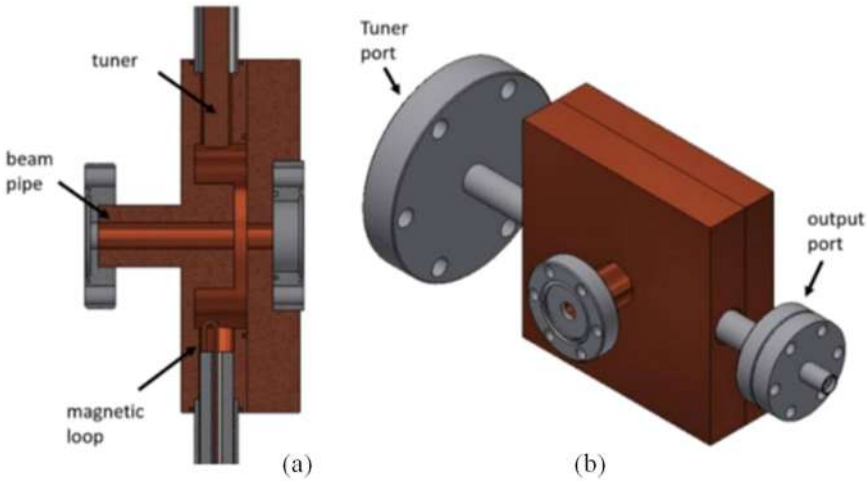

FIG. 8. Cavity prototype mechanical drawing: section (a) and complete layout (b).

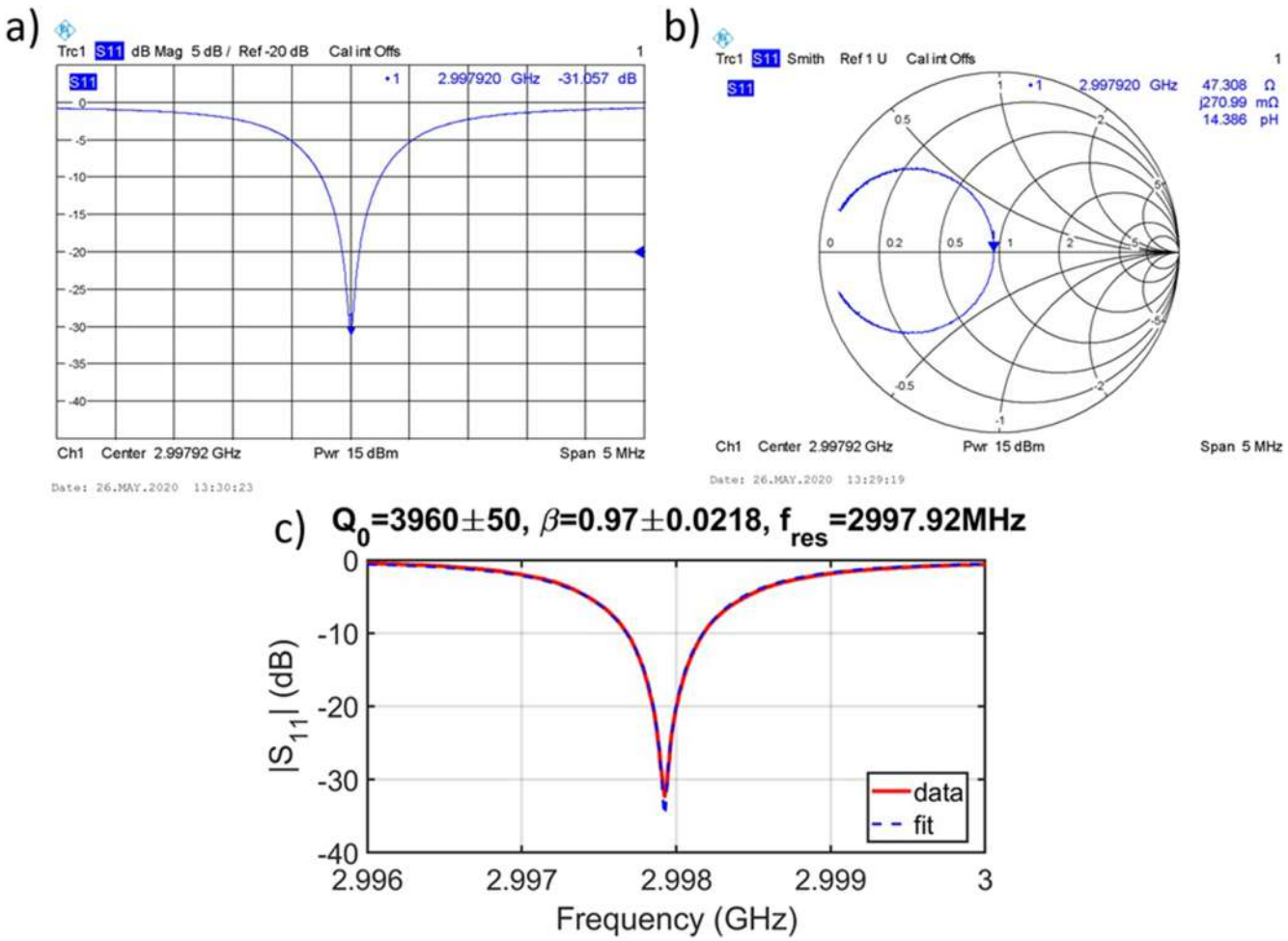

FIG. 9. RF measurement results: reflection coefficient (a), Smith chart (b), and data fitting of the reflection coefficient (c).

TABLE III. RF parameters of the cavity prototype compared to the design values.

Parameter	Unit	Design value	Measured value
f_0	MHz	2997.92	2997.92
Q_0	···	4257	3960
Q_{load}	···	2129	2010
β	···	1	0.97
τ	ns	225	213
R_S/Q_0	Ohm	60	···

realized brazing together two previously machined parts. On one side of the detector, the tuning port has been implemented to connect a tuning system similar to the one employed in the SCDTL structures, and on the other side is the magnetic pickup with the output coaxial port. The cavity is connected to the beamline with two CF16 flanges.

Before the installation, the prototype has been vacuum tested and characterized by means of cold RF measurements in vacuum, obtaining the main RF parameters S11, Q_0, and β. The reflection coefficient and the Smith chart obtained with the network analyzer are shown in Fig. 9.

During this phase, the pickup insertion depth has been adjusted by changing the thickness of the copper vacuum gasket. Using a data fitting routine, the unloaded quality factor and coupling coefficient of the cavity have been calculated. At the end of the regulation, the coupling coefficient was 0.97. Table III reports the principal RF parameters of the cavity obtained from RF measurements. The value of the filling time, calculated as $\tau = 2Q_{load}/\omega$ applying the measured cavity parameters, is $\tau = 213$ ns. This value is much smaller than the pulse length, as requested to obtain a faithful representation of the beam pulse.

VI. CHARACTERIZATION TEST WITH THE PROTON BEAM

A. Preliminary tests in air

All the characterization measurements have been carried out at the exit of the SCDTL-4 module before the installation of the second SCDTL section. Preliminary tests were performed with the detector installed in air[11] with the aim of evaluating the dynamic range capability. In these measurements, the cavity has been placed in air, following a calibrated current transformer and ionization chamber (Fig. 10), to measure independently the pulse current values in an intensity range between 2 and 45 μA.

The cavity response was characterized by connecting it to a Rohde & Schwarz ZVL-6 Vector Network Analyzer (VNA). The ZVL-6 was connected to the cavity with a 1.5 m coaxial cable having a characterized attenuation of 1.2 dB at 3 GHz. Cavity correct tuning was checked before power measurement, and then the instrument was switched to spectrum analysis without disconnecting the cable. Two measurement classes were carried out: spectrum analysis and pulse envelope analysis.

The maximum-hold trace mode has been used to reconstruct the pulse spectrum envelope, asynchronously acquiring a large number of pulses. The spectrum has two sidelobes [Fig. 11(a)] separated

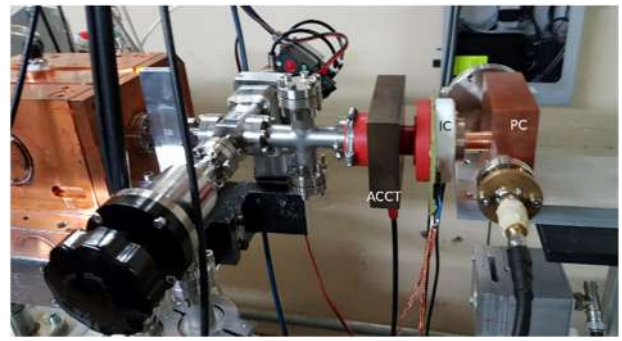

FIG. 10. Passive cavity (PC) prototype at the linac exit installed after other beam diagnostic instrumentation: a current transformer (ACCT) and an ionization chamber (IC) during the tests in air.

by about 50 MHz due to the harmonic component of the 425 MHz injector frequency modulating the beam, as expected according to the discussion in Sec. II A. It is noteworthy to say that the sidelobe structure of the pulse is attenuated due to the filtering effect of the cavity itself.

The pulse envelope analysis has been carried out centering the spectrum analyzer at 2997.92 MHz and set its operation to zero span [Fig. 11(b)].

Cavity power measurements at different beam currents are reported in Fig. 12, where they are compared with the analytical model of Eq. (1) with the measured parameters of Table III. The observed output signal level covers the −38 to −10 dBm range, lower than that expected from the model. This discrepancy can be due to not easily quantifiable uncertainties both in parameter evaluation and in measurement accuracy, despite efforts in the measurement procedures and calibrations. However, even with this systematic discrepancy, the detector behavior is well reproduced by the expected functional form through a simple scaling factor that has been estimated as 0.65 ± 0.06.

The measured dynamic range is then taken into account in the design of the electronic chain that integrates the real-time monitoring detection of the passive cavity into the accelerator control system.

The RF signal generated at the output port of the cavity is frequency down converted and processed to allow deriving the current profile information.

In the first prototype, a two branch circuit, simultaneously providing measurements for low and high currents, which employed two zero-bias Schottky diodes inserted in two different gain paths, had been used to cover the 40 dB wide dynamic range.[11] However, the still unacceptable precision in the full dynamic range and the complexity and the cost of such a system led to the development of a different detection system.

B. Detection system for in-vacuum characterization

Following the preliminary test performed in air, the current monitor prototype has been integrated in its final position in the machine layout. Hence, the cavity has been connected to the beam pipe and pumped down to vacuum. The resonant frequency of the cavity has been adjusted acting on the tuner.

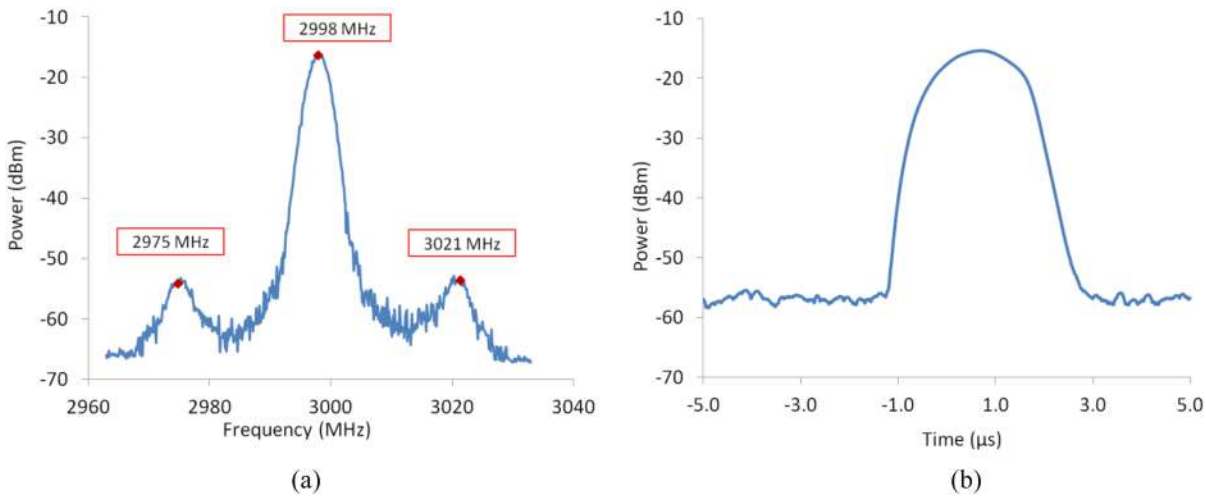

FIG. 11. Vector network analyzer measurements at 29 μA: (a) spectrum of the output cavity signal and (b) pulse envelope.

New spectrum analyzer measurements of the cavity response confirmed an almost 40 dB of dynamic range.

For these measurements, a different detection system (Fig. 13) was adopted to overcome the limitations of the previous scheme reported in Ref. 11. The current signal is extracted from the envelope of the cavity output using the ZX47-60+ power detector manufactured by Mini-Circuits. The detector consists of a logarithmic envelope-detecting amplifier characterized by a wide dynamic range, extending from −60 to −5 dBm at 3 GHz, with a nominal transducer gain of −25 mV/dB and a log-conformance of ±1 dB within that range. The video output of the power detector consists of an analog voltage in the 2.10–0.5 V range, varying linearly with the input power expressed in dB. It also outputs an analog voltage signal proportional to its temperature to compensate temperature-dependent variation (2 mV/C) on the video output.

The intended use of the ZX47-60+ detector is in transmit power control loops in RF systems to stabilize the output of the RF power amplifiers and is not designed to provide an accurate representation of the envelope of the input signal during large transients. This is particularly evident in the asymmetry between the rise and fall times that are 400 and 10 ns, respectively. As a consequence, the current signal is distorted and presents a long tail, longer than the actual decay of the field in the cavity detector.

The available documentation also does not report the video bandwidth. A reasonable estimation of it can be deduced from the fall time (tf) information,

$$\mathrm{BW} = 0.35/\mathrm{tf} = 0.35/\left(10^{*}10^{-9}\right) = 35\ \mathrm{MHz}.$$

The ZX47-60+ power detector is placed next to the cavity in a shielded aluminum box connected to it with a 1 m long coaxial

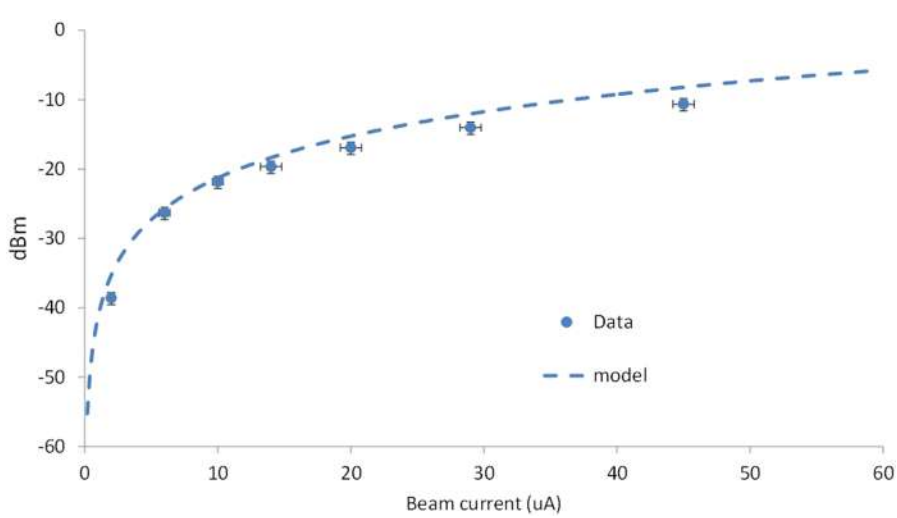

FIG. 12. Cavity output power vs pulse current: measurements (dots) and model (line).

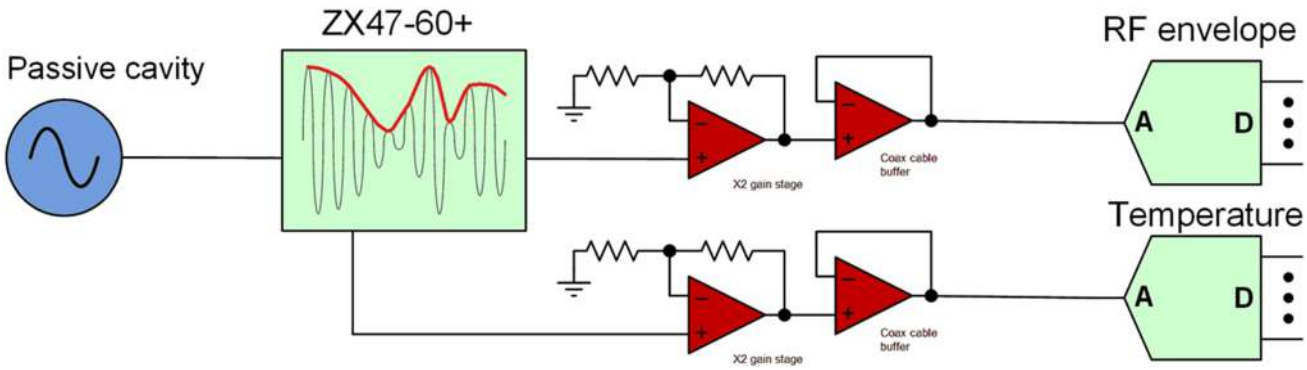

FIG. 13. Detection system used in the measurements with the passive cavity in vacuum.

cable in the accelerator bunker. Signal acquisition and processing is performed in the control room. The communication between the two environments is guaranteed by 50 Ω coaxial cable with matched terminations.

The ZX47 video and temperature outputs have minimum impedance requirements of 100 and 2000 Ω, respectively, and cannot be connected directly to 50 Ω systems.

To overcome this limitation, front-end electronics has been developed, consisting of a gain stage followed by a high current buffer, as shown in Fig. 13. The front-end electronics is hosted in the detector box.

The gain stage sets the load impedance for the detector ports (1 kΩ for the video output and 10 kΩ for the temperature output), provides a gain of 2 V/V, and sets the system bandwidth to 12 MHz. The high current buffer sets the output impedance to 50 Ω and is able to source or sink up to 250 mA. Front-end electronics provides an overall gain of 1 V/V on a load impedance of 50 Ω and sets the system bandwidth to 12 MHz. This value, lower than the one of the detector alone, is sufficient to correctly detect the power level of the flattop of the TOP-IMPLART current pulses that have widths ranging from 1 to 5 μs.

The full acquisition chain (i.e., power detector, amplifier, cable, and scope) has been characterized using two different precision RF sources, both in CW and in pulsed mode, to obtain an experimental input power (P_{in}) vs output voltage (V_{out}) curve in the range of −46 to 7 dBm. The output voltage is calculated as the difference between the flattop and the pedestal and is a positive quantity. The uncertainties taken into account in this characterization are the input power reproducibility, estimated to be $\Delta P = \pm 0.2$ dBm, and the oscilloscope binning resolution and DC gain accuracy ($\Delta V = \pm 10$ and ± 38 mV, respectively). The best fit of the experimental data is

$$V_{out@1M\Omega} = M_{cal} * P_{in} + Q_{cal}, \tag{4}$$

with $M_{cal} = 49.3 \pm 0.1$ mV/dBm and $Q_{cal} = 3221 \pm 3$ mV; V_{out} is expressed in mV, and P_{in} is expressed in dBm.

The system was then tested at different current levels in order to perform a cross-calibration of the passive RF cavity with the already installed diagnostic devices: the ACCT and Faraday cup. The output current has been changed varying the voltage on the Einzel lens placed in the injector. Figure 14 shows the output signal from the passive cavity detection system for two different current values

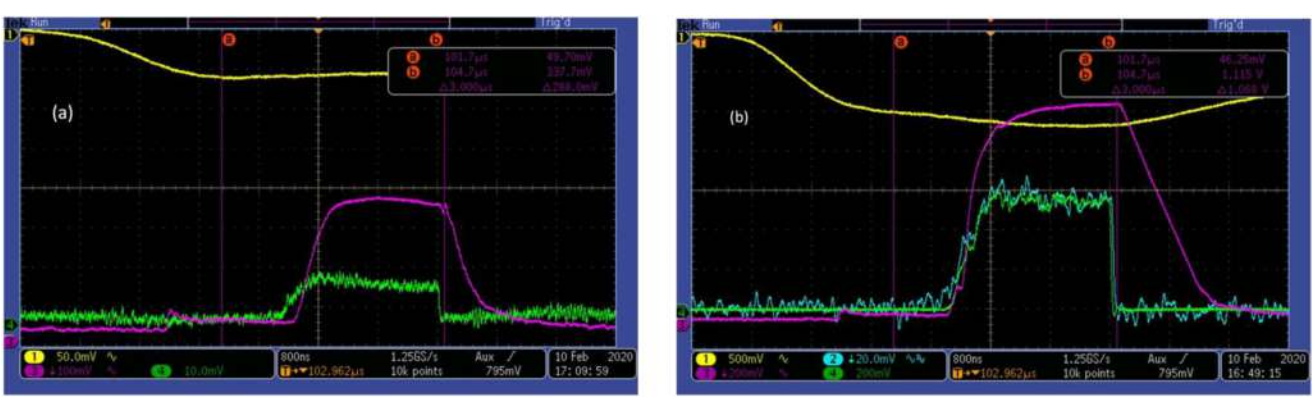

FIG. 14. Beam current profile measurement at the end of the fourth SCDTL structure reads with an oscilloscope for two different values of the current injected into SCDTL structures: (a) AC transformer at SCDTL-1 input (yellow, scale = 50 μA/div), Faraday cup (green, scale = 0.5 μA/div), and passive cavity (purple). (b) AC transformer at SCDTL-1 input (yellow, scale = 500 μA/div), Faraday cup (green, scale = 10 μA/div), current transformer (blue, scale = 10 μA/div), and passive cavity (purple).

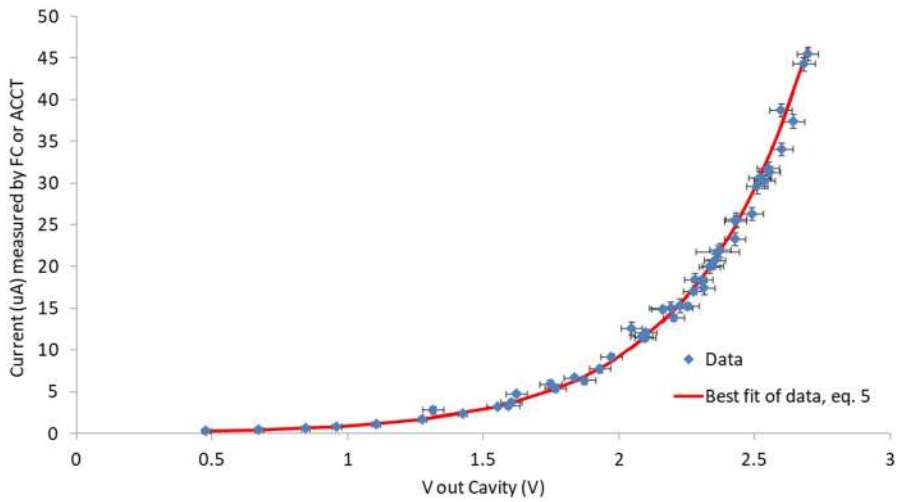

FIG. 15. Calibration curve [Eq. (5)] and beam pulse vs detector output voltage data.

compared to the signal of the Faraday cup and current transformer at high intensity and only with the signal of the Faraday cup at low intensity (where the current transformer is outside its working range). In the cavity traces, a non-zero signal less than 100 mV of amplitude is visible about 2 μs before the actual beam signal at the RF power system switching on. This effect, which limited the detector operating range, has been then removed by putting the amplifier circuit in the shielded aluminum box.

Figure 15 reports the beam current intensity as retrieved by both the detection systems described above vs the measured values of the output signal of the cavity in volts. They have been acquired by the oscilloscope, simultaneously recording the average value on the plateau for the traces of Faraday cup, ACCT, and passive cavity. The data follow an exponential law, as expected, since the ZX47-60+ power meter output voltage is linear with the logarithm of the input power according to Eq. (4). The errors on the measured data take into account the uncertainties for different instrumentations depending on the combined binning resolution and DC gain accuracy of the scope used for the data acquisition. The calibration uncertainties have also been taken into account, but their contribution is negligible with respect to the voltage uncertainty.

The best fit of the measured data gives the following empirical calibration curve of the beam current vs the measured voltage shown in Fig. 16 as a solid line:

$$I[\mu A] = 0.086^{*} \exp\left(2.33^{*} V_{meas}\right), \tag{5}$$

with V_{meas} expressed in volt.

The impact of the measured voltage uncertainty on the beam current evaluated with this calibration model is given by the relation

$$\delta I/I = 2.33^{*} \delta V, \tag{6}$$

with δV expressed in volt.

To the typical oscilloscope acquisition setting $\delta V \approx 40$ mV corresponds a beam current relative uncertainty of ±9%, which is adequate to monitor the beam intensity stability pulse to pulse and could be further improved with a dedicated, higher accuracy digitization system.

Figure 16 shows the passive cavity in its final position in the inter-module space between SCDTL-4 and SCDTL-5 together with a vacuum valve and an ACCT placed between two PMQs.

Presently, there is no temperature control on the passive cavity in contrast to the SCDTL accelerating structures, which are provided with a thermo-regulator system and operated within a temperature stability of ±0.02 °C (Ref. 2). However, while the SCDTL structures have Q_0 values up to ≈11 000, the passive cavity, thanks to its lower Q_0 (≈4000), is less prone to thermal detuning. From Eqs. (1) and (3), it can be calculated that a 50 kHz detuning, induced by a 1 °C temperature variation, only results in a power variation of about 0.5%, which is negligible compared to the other uncertainties we accounted for in our experimental setup. Nevertheless, the resonant frequency of the passive cavity was checked before and after all measurements reported in this paper to ensure no significant temperature variation had occurred.

To ensure long term stability and reliability of the device, even at a higher repetition frequency (50–100 Hz), we plan to acquire the temperature readout of the power detector and also equip the passive cavity with a cooling system.

FIG. 16. Passive cavity (PC) placed in the drift space between SCDTL-4 and SCDTL-5.

VII. CONCLUSIONS

This paper reports the design and test of a very compact beam current detector with a wide dynamic range for the proton therapy linear accelerator. Such real-time, nondestructive systems play a key role in a medical accelerator because they allow us to monitor the status of the machine and beam charge stability during patient treatment. Thus, they could represent a useful integration to the standard dose delivery control system based on the calibrated ionization chamber.

The proposed detector is based on a passive RF cavity working in vacuum and operating in the TM010 mode at the same repetition frequency of the beam micro-bunches. A prototype has been realized and integrated in the TOP-IMPLART linac layout. Two different tests have been performed in air and in vacuum, in order to characterize separately the response of the passive cavity alone, by means of a spectrum analyzer, and then the complete device including a simple and cost effective power detection system. The test results definitively demonstrate the reliability and suitability of such diagnostics for medical proton linacs.

Given the satisfactory results of the first passive RF cavity prototype, we plan to install other passive RF monitors at each intersection between the accelerator modules to additionally provide online monitoring of the beam transmission throughout the linac, offering useful information on the machine status to the operators.

ACKNOWLEDGMENTS

This work was funded by the Innovation Department of Regione Lazio Government (Italy) under Grant No. CUP:I11J10000420002.

AUTHOR DECLARATIONS

Conflict of Interest

The authors have no conflicts of interest to disclose.

DATA AVAILABILITY

The data that support the findings of this study are available from the corresponding author upon reasonable request.

REFERENCES

[1] C. Ronsivalle, M. Carpanese, C. Marino, G. Messina, L. Picardi, S. Sandri, E. Basile, B. Caccia, D. M. Castelluccio, E. Cisbani, S. Frullani, F. Ghio, V. Macellari, M. Benassi, M. D'Andrea, and L. Strigari, "The TOP-IMPLART project," Eur. Phys. J. Plus **126**, 68 (2011).

[2] L. Picardi, A. Ampollini, G. Bazzano, E. Cisbani, F. Ghio, R. M. Montereali, P. Nenzi, M. Piccinini, C. Ronsivalle, F. Santavenere, V. Surrenti ,E. Trinca, M. Vadrucci, and E. Wembe Tafo, "Beam commissioning of the 35 MeV section in an intensity modulated proton linear accelerator for proton therapy," Phys. Rev. Accel. Beams **23**, 020102 (2020).

[3] N. Esplen, M. S. Mendonca, and M. Bazalova-Carter, "Physics and biology of ultrahigh dose-rate (FLASH) radiotherapy: A topical review," Phys. Med. Biol. **65**, 23TR03 (2020).

[4] C. Ronsivalle, A. Ampollini, G. Bazzano, P. Nenzi, L. Picardi, V. Surrenti, E. Trinca, and M. Vadrucci, "The TOP-IMPLART linac: Machine status and experimental activity," in *Proceedings of the 18th International Particle Accelerator Conference (IPAC'17)* (2017), pp. 4669–4672.

[5] G. Bazzano, A. Ampollini, F. Cardelli, F. Fortini, P. Nenzi, G. B. Palmerini, L. Picardi, L. Piersanti, C. Ronsivalle, V. Surrenti, E. Trinca, M. Vadrucci, and M. Sabatini, "Radiation testing of a commercial 6-axis MEMS inertial navigation unit at ENEA Frascati proton linear accelerator," Adv. Space Res. **67**(4), 1379 (2021).

[6] A. Ampollini, E. Basile, G. Bazzano, E. Cisbani, C. De Angelis, S. Della Monaca, F. Ghio, F. Giuliani, M. Lucentini, P. Nenzi, C. Placido, L. Picardi, C. Ronsivalle, F. Santavenere, A. Spurio, V. Surrenti, and M. Vadrucci, "Recombination effects in the ionization chambers dose delivery monitor of the TOP-IMPLART proton beam," J. Phys.: Conf. Ser. **1561**(1), 012008 (2020).

[7] D. Brandt, "CERN accelerator school, beam diagnostics," CERN Yellow Reports: School Proceedings Report No. CERN2009-005, November 2009, Dourdan, France, 28 May–6 June 2008.

[8] A. Leggieri, D. Passi, F. di Paolo, A. Ciccotelli, S. De Stefano, F. Marangoni, and G. Felici, "Real-time beam monitor for charged particle medical accelerators," IEEE Trans. Nucl. Sci. **63**(2), 869 (2016).

[9] T. R. Pusch, F. Frommberger, W. C. A. Hillert, and B. Neff, "Measuring the intensity and position of a pA electron beam with resonant cavities," Phys. Rev. Accel. Beams **15**, 112801 (2012).

[10] R. G. Carter, "Calculation of the properties of reentrant cylindrical cavity resonators," IEEE Trans. Microwave Theory Tech. **55**(12), 2531 (2007).

[11] P. Nenzi, A. Ampollini, G. Bazzano, F. Cardelli, L. Picardi, L. Piersanti, C. Ronsivalle, V. Surrenti, and E. Trinca, "Development of a passive cavity beam intensity monitor for pulsed proton beams for medical applications," in Proceedings of the 8th International Beam Instrumentation Conference MOCO02, Malmö, Sweden, 8–12 September 2019.